Carcinogenesis, 2021, Vol. 42, No. 2, 272–284

doi:10.1093/carcin/bgaa095
Advance Access publication September 11, 2020
Original Article

ORIGINAL ARTICLE

Targeting of BCR-ABL1 and IRE1α induces synthetic lethality in Philadelphia-positive acute lymphoblastic leukemia

Margherita Vieri[1], Christian Preisinger[2], Mirle Schemionek[1], Azam Salimi[1], John B.Patterson[3], Afshin Samali[4,5], Tim H.Brümmendorf[1], Iris Appelmann[1,*,†] and Behzad Kharabi Masouleh[1,†]

[1]Department of Hematology, Oncology, Hemostaseology and Stem Cell Transplantation and [2]Proteomics Facility, Interdisciplinary Centre for Clinical Research, RWTH Aachen University Medical School, Aachen 52074, Germany, [3]Fosun Orinove PharmaTech Inc., 3537 Old Conejo Rd., Suite 104, Newbury Park, CA 91320, USA, [4]Apoptosis Research Centre and [5]Department of Biochemistry, National University of Ireland, Galway H91 TK33, Ireland

*To whom correspondence should be addressed. Tel: +49(0)241-8037358; Fax: +49(0)241 8082449; Email: iappelmann@ukaachen.de
†These authors contributed equally to this work.

Abstract

BCR-ABL1-positive acute lymphoblastic leukemia (ALL) cell survival is dependent on the inositol-requiring enzyme 1 alpha (IRE1α) branch of the unfolded protein response. In the current study, we have focused on exploring the efficacy of a simultaneous pharmacological inhibition of BCR-ABL1 and IRE1α in Philadelphia-positive (Ph^+) ALL using tyrosine kinase inhibitor (TKI) nilotinib and the IRE1α inhibitor MKC-8866. The combination of 0.5 µM nilotinib and 30 µM MKC-8866 in Ph^+ ALL cell lines led to a synergistic effect on cell viability. To mimic this dual inhibition on a genetic level, pre-B-cells from conditional $Xbp1^{+/fl}$ mice were transduced with a BCR-ABL1 construct and with either tamoxifen-inducible cre or empty vector. Cells showed a significant sensitization to the effect of TKIs after the induction of the heterozygous deletion. Finally, we performed a phosphoproteomic analysis on Ph^+ ALL cell lines treated with the combination of nilotinib and MKC-8866 to identify potential targets involved in their synergistic effect. An enhanced activation of p38 mitogen-activated protein kinase α (p38α MAPK) was identified. In line with this findings, p38 MAPK and, another important endoplasmic reticulum-stress-related kinase, c-Jun N-terminal kinase (JNK) were found to mediate the potentiated cytotoxic effect induced by the combination of MKC-8866 and nilotinib since the targeting of p38 MAPK with its specific inhibitor BIRB-796 or JNK with JNK-in-8 hindered the synergistic effect observed upon treatment with nilotinib and MKC-8866. In conclusion, the identified combined action of nilotinib and MKC-8866 might represent a successful therapeutic strategy in high-risk Ph^+ ALL.

Introduction

The endoplasmic reticulum (ER) orchestrates the production, control and correct folding of cellular proteins and represents the key cellular organelle in maintaining protein homeostasis (proteostasis) (1). Disturbances such as hypoxia or nutrient deprivation can lead to 'ER stress', which, in turn, triggers surveillance systems, such as the unfolded protein response (UPR) to shield cells against such stress. The UPR can in this regard respond either in an acute and reversible manner as a reliever of stress or in a chronic and terminal manner as an inducer of apoptosis. Cancer cells have shown to be critically dependent on a well-developed ER system (2,3). Within the ER, three branches act as key players of the UPR, namely inositol-requiring enzyme

Received: November 29, 2019; **Revised:** August 7, 2020; **Accepted:** September 9, 2020

Abbreviations

4OHT	4-hydroxy-tamoxifen
ALL	acute lymphoblastic leukemia
ANOVA	analysis of variance
ATF6α	activating transcription factor 6 alpha
DMSO	dimethyl sulfoxide
eIF2AK3	eukaryotic translation initiation factor 2-alpha kinase 3
ER	endoplasmic reticulum
FACS	fluorescence-activated cell sorting
IRE1α	inositol-requiring enzyme 1 alpha
JNK	c-Jun N-terminal kinase
MAPK	mitogen-activated protein kinase
mRNA	messenger RNA
Ph⁺	Philadelphia positive
PBS	phosphate-buffered saline
PI	propidium iodide
RNase	endoribonuclease
TKI	tyrosine kinase inhibitor
UPR	unfolded protein response
XBP1	X-box binding protein 1

1 alpha (IRE1α), eukaryotic translation initiation factor 2-alpha kinase 3 (eIF2AK3, also known as PERK) and activating transcription factor 6 alpha (ATF6α) (4).

IRE1α contains an endoribonuclease (RNase) and a kinase domain. The RNase domain of IRE1α is essential for the splicing of the X-box binding protein 1 (*XBP1*) messenger RNA (mRNA) (5) and subsequently for the production of a highly transcriptionally active protein (XBP1s). The kinase domain promotes an additional molecular response (6) eventually leading to the activation of upstream kinases for c-Jun N-terminal kinase (JNK) and p38 mitogen-activated protein kinase (p38 MAPK), initiating cell death (7).

Pharmacological targeting of the sole RNase domain of IRE1α appears to be a very promising preclinical anticancer strategy in a variety of model systems, for example, multiple myeloma (8), chronic lymphocytic leukemia (9), breast cancer (10), pancreatic cancer (11), acute myeloid leukemia (12) and acute lymphoblastic leukemia (ALL) (13).

In this work, we followed up our previous discoveries on the role of the UPR in Philadelphia-positive ALL (Ph⁺ ALL), a hematologic malignancy driven by the BCR-ABL1 oncoprotein resulting from the Philadelphia translocation t(9;22). We already showed that homozygous deletion of XBP1 was sufficient to cause apoptosis and cell cycle arrest in genetic mouse models of ALL (13), while the therapeutic link between BCR-ABL1 kinase activity and IRE1α signaling remained unclear.

Ph⁺ ALL represents a genetically defined subset of ALL with very poor clinical outcome (14), particularly if allogeneic stem cell transplantation cannot be performed due to old age or comorbidities of the affected patient or due to a lacking suitable donor. Here, we identified a promising pharmacological strategy to treat Ph⁺ ALL by combining the inhibition of BCR-ABL1 [via the tyrosine kinase inhibitor (TKI) nilotinib] and IRE1α (via the IRE1α RNase domain inhibitor MKC-8866).

Material and methods

Human cell lines

Human cell lines SUP-B15 and TOM-1 were originally obtained from DSMZ, Braunschweig, Germany. Cell lines were authenticated using Multiplex Cell Authentication by Multiplexion, Heidelberg, Germany, last in November 2019 as described by Castro *et al.* (15). The single nucleotide polymorphism profiles matched known profiles. Human leukemia cells were cultured in RPMI medium (RPMI-1640, Invitrogen®) with GlutaMAX containing 10% fetal bovine serum, 100 IU/ml penicillin and 100 μg/ml streptomycin at 37°C in a humidified incubator with 5% CO_2. Viability was determined with methylene blue exclusion staining or with propidium iodide (PI) as described in the paragraph 'Flow cytometry'.

Extraction of bone marrow cells from mice

All experiments involving the use of animals were conducted according to the German Animal Protection legislation. Bone marrow cells were extracted from young age-matched heterozygous mice with conditional *Xbp1* background (*Xbp1*$^{+/fl}$). We obtained the bone marrow cells by flushing cavities of femur and tibia with phosphate-buffered saline (PBS). After filtration through a 0.45 μm filter and depletion of erythrocytes using a lysis buffer (BD PharmLyse, BD Biosciences®), washed cells were either frozen for storage or subjected to further experiments.

Mouse model of human Ph⁺ ALL

We collected bone marrow cells from the abovementioned mice and transduced them using a BCR-ABL1 retrovirus in the presence of 10 ng/ml interleukin-7 (Peprotech®). BCR-ABL1-transformed pre-B-cells were either treated with the drugs mentioned in the following paragraph 'Inhibitor studies' or transduced with (Tamoxifen) inducible empty vector controls and cre and used as a genetic model of BCR-ABL1⁺ ALL. The deletion was induced adding 1 μM 4-hydroxy-tamoxifen (4OHT). An overview of the plasmids used is shown in Supplementary Table 1.

Retroviral transduction

We performed transfections of retroviral constructs and their corresponding empty vector controls using calcium phosphate precipitate as transfection reagents with Dulbecco's Modified Eagle Medium media (Gibco®) and Plat-E cells as packaging cells. Calcium phosphate precipitate containing the plasmid of interest was distributed on Plat-E culture and incubated for 16 h. Twenty-four hours later, the virus supernatants were harvested, filtered through a 0.45 μm filter and loaded by centrifugation (2000 *g* for 120 min at 32°C) on 50 μg/ml RetroNectin (Takara®) coated non-tissue six-well plates. 2–3 × 10^6 pre-B-cells were transduced per well by centrifugation at 600 *g* for 30 min and maintained at 37°C with 5% CO_2.

Quantitative real-time PCR

Total RNA from cells was extracted using Trizol reagent (Ambion®) followed by chloroform extraction. Complementary DNA was generated using random hexamers and the M-MLV Reverse Transcriptase (Invitrogen®). Quantitative real-time PCR was performed with the SYBRGreen mix (Invitrogen®) and the ABI7500fast real-time PCR system (Applied Biosystems®) according to standard PCR conditions. Primers for quantitative real-time PCR are listed in Supplementary Table 2.

Inhibitor studies

MKC-8866 was obtained from Mannkind®, Valencia, CA, dissolved in dimethyl sulfoxide (DMSO) and stored at –20°C for further experiments. Nilotinib, imatinib and BIRB-796 were obtained from LC Labs® and JNK-in-8 from SelleckChem®. All drugs were dissolved in DMSO and stored at –20°C for further experiments. The cells were treated with the inhibitors for specific time points as mentioned in the according experiments.

Flow cytometry

Cells were washed and resuspended in PBS with PI (0.2 μg/ml, BD Biosciences®) as a dead cells marker. For proliferation assay in Ph⁺ ALL cell lines, 5(6)-Carboxyfluorescein diacetate N-succinimidyl ester (CFSE) solution (Sigma-Aldrich®, 500 nM in PBS) was used, in which cells were incubated for 15 min in room temperature protected from light and then washed twice with PBS. CFSE is a fluorescent dye that irreversibly binds to the cytoplasm, allowing the cells to be followed through cell divisions. After labeling, the cells were treated with the mentioned inhibitors for specific time points as reported in the according experiments.

Cell cycle analysis was performed as follows. 0.5 × 10^6 cells were resuspended in saline-solution containing glucose 1.1 g/L, NaCl 8 g/L, KCl 0.4 g/L, $Na_2HPO_4 \cdot 2H_2O$ 0.2 g/L, KH_2PO_4 0.15 g/L, and EDTA 0.2 g/L, permeabilized

using ethanol 90% and then stained with a solution of PI 10 and 25 µg/ml RNase for 1 h. The cells were finally analyzed by fluorescence-activated cell sorting (FACS; BD Accuri C6®). The entire procedure was performed at 4°C. The analysis for CFSE and cell cycle assays was gated on viable cells that were identified based on scatter morphology.

Western blotting and mass spectrometry analysis

The methods used are described in detail in the Supplementary Material.

Data availability

The mass spectrometry proteomics data have been deposited to the ProteomeXchange Consortium (http://proteomecentral.proteomexchange.org) via the PRIDE (16) partner repository with the data set identifier PXD012024.

Statistical analysis

Every figure shows the mean results of three independent experiments ± standard deviation, unless representative figures are shown, which are labeled as such. Statistical analyses were performed with GraphPad Prism (GraphPad Software®). The unpaired Student's *t*-test was applied for single comparisons and analysis of variance (ANOVA; one- or two-way) was used for multiple comparison analysis, employing the Bonferroni multiple comparison post-test. The specific test used is reported in the legend of each figure. *P* values less than 0.05 were considered statistically significant.

Bliss formula calculation

Drug additivity or synergy was determined by using the criteria described by Greco *et al.* (17). Synergy is calculated in Figure 2A using the Bliss independence model, defined by the equation: $E_{xy} = (E_x + E_y) - (E_x \times E_y)$. E_{xy} is the additive effect of drugs *x* and *y* as predicted by their observed individual effects (E_x and E_y). The percentage of dead cells was used to evaluate the effect of each drug used alone (E_x and E_y) or in combination with each other (experimental value). We stated both drugs additive when the experimental value obtained was equal to E_{xy}, synergistic when it was $>E_{xy}$ and antagonists when it was $<E_{xy}$. The unpaired Student's *t*-test was used to determine statistical significance.

Results

The IRE1α inhibitor MKC-8866 has antiproliferative effects in Ph$^+$ ALL

We have shown previously that the UPR might be an important target in high-risk ALL using early preclinical compounds (13). In this study, we tested the small molecule, MKC-8866, designed to specifically inhibit the RNase domain of IRE1α. MKC-8866 has significantly improved pharmacodynamics, pharmacokinetics and reduced toxicity compared with previously tested molecules with the same targeted activity, such as STF-083010 or A106 (18,19). In that same aforementioned study (13), oncogenic BCR-ABL1 influenced the function of IRE1α, resulting in increased expression and activity of XBP1 in BCR-ABL1$^+$ ALL cells compared with normal B-cell precursors. Based on this finding, we tested the hypothesis that dual pharmacological targeting of IRE1α–XBP1 axis and BCR-ABL1 could be beneficial, perturbing different nodes of a same pivotal pathway for ALL survival. In order to determine the range of efficacy of MKC-8866, we performed titration assays in the human Ph$^+$ ALL cell lines SUP-B15 and TOM-1 (Figure 1A). For SUP-B15, an half maximal inhibitory concentration IC50 of 69.0 ± 1.1 µM (mean ± standard deviation) was calculated, whereas, for TOM-1, the IC50 resulted to be 26.5 ± 3.7 µM. In order to test MKC-8866 in combination with an appropriate concentration of nilotinib, we performed the same assays with this compound (Figure 1B), evidencing an IC50 of 1.2 ± 0.02 µM for SUP-B15 and 0.61 ± 0.04 µM for TOM-1. To better evaluate the efficacy of dual treatment with MKC-8866 and nilotinib on both a treatment-sensitive cell line (TOM-1) and on a more resistant one, namely SUP-B15, we kept the conditions unchanged in the following experiments using nilotinib at the concentration of 0.5 µM and MKC-8866 at 30 µM. The inhibition of the RNase activity of IRE1α using MKC-8866 alone or in combination with nilotinib was confirmed in both cell lines by the significantly decreased mRNA levels of *XBP1s*. Nilotinib used as single treatment was also able to decrease *XBP1s* mRNA levels. However, this effect was observed in TOM-1 but not in SUP-B15 cells (Figure 1C).

Treatment with MKC-8866 is synergistic with TKI in Ph$^+$ ALL

Using human Ph$^+$ ALL cell lines SUP-B15 and TOM-1 as models, we tested the biological effects on the proliferation of combining TKI nilotinib and IRE1α inhibitor MKC-8866. Staining the cells with CFSE showed a non-significant reduction in the proliferation rate upon application of single agents MKC-8866 and nilotinib and, remarkably, a significant decrease upon combined targeting (Figure 1D and Supplementary Figure 1A and C). In addition, both single and dual treatments with MKC-8866 and nilotinib induced mild cell cycle alterations: although the G1 phase population was not affected, cells in S phase were slightly increased upon combined treatment and those in G2-M phase were significantly reduced, even when compared with monotherapies (Figure 1E).

The most important observation to emerge from our experiments was that dual therapy with nilotinib and MKC-8866 caused a substantial increase of cell death of Ph$^+$ ALL cells (Figure 2A). Using the Bliss independence formula (20), a synergistic effect was verified (Figure 2A, bottom right). Further tests were carried out using the TKI imatinib in combination with MKC-8866. Here, we could show that the combination of MKC-8866 and imatinib 10 µM had similar effects on SUP-B15 and TOM-1, with a significant reduction of viability after 3 days of treatment (Supplementary Figure 2A) and a reduction in the proliferation rate (Supplementary Figure 1B and 2B). *XBP1* mRNA levels decreased upon treatment with MKC-8866 alone or in combination with imatinib as shown in Supplementary Figure 2C. Unlike nilotinib, however, single treatment with imatinib failed to decrease *XBP1s* levels in TOM-1. It is interesting to note that the same treatment regimen was ineffective in two non-Ph$^+$ ALL cell lines, such as ETV-RUNX1$^+$ cell line REH and the MLL-AF4$^+$ cell line SEM (Supplementary Figure 3). Overall, our data show that combined IRE1α and BCR-ABL1 targeting irreversibly reduces the viability of human Ph$^+$ ALL cells.

Heterozygous deletion of *Xbp1* is sufficient to render BCR-ABL1$^+$ ALL cells sensitive toward TKI treatment

Since pharmacological inhibition by MKC-8866 causes a reduction of *XBP1* expression (Figure 1B), we aimed to genetically dissect the mechanism at the basis of TKI's and MKC-8866's synergism using bone marrow B-cell precursors from *Xbp1*$^{+/fl}$ mice instead of *Xbp1*$^{fl/fl}$ to model human BCR-ABL1 ALL with reduced, but not abrogated, XBP1 signaling (21). Murine BCR-ABL1$^+$ ALL cells transduced with cre-ER^{T2}-puro or the empty vector were treated with both imatinib and nilotinib alone or together with 4OHT to induce heterozygous deletion of *Xbp1*. Supporting the notion of increased sensitivity, heterozygous deletion of *Xbp1* significantly enhanced the effect of both imatinib and nilotinib in *Xbp1*$^{+/fl}$ BCR-ABL1 cre-ER^{T2}-puro ALL (Figure 2B and C). It is also important to note that both TKIs further reduced the expression of *Xbp1* on the mRNA level

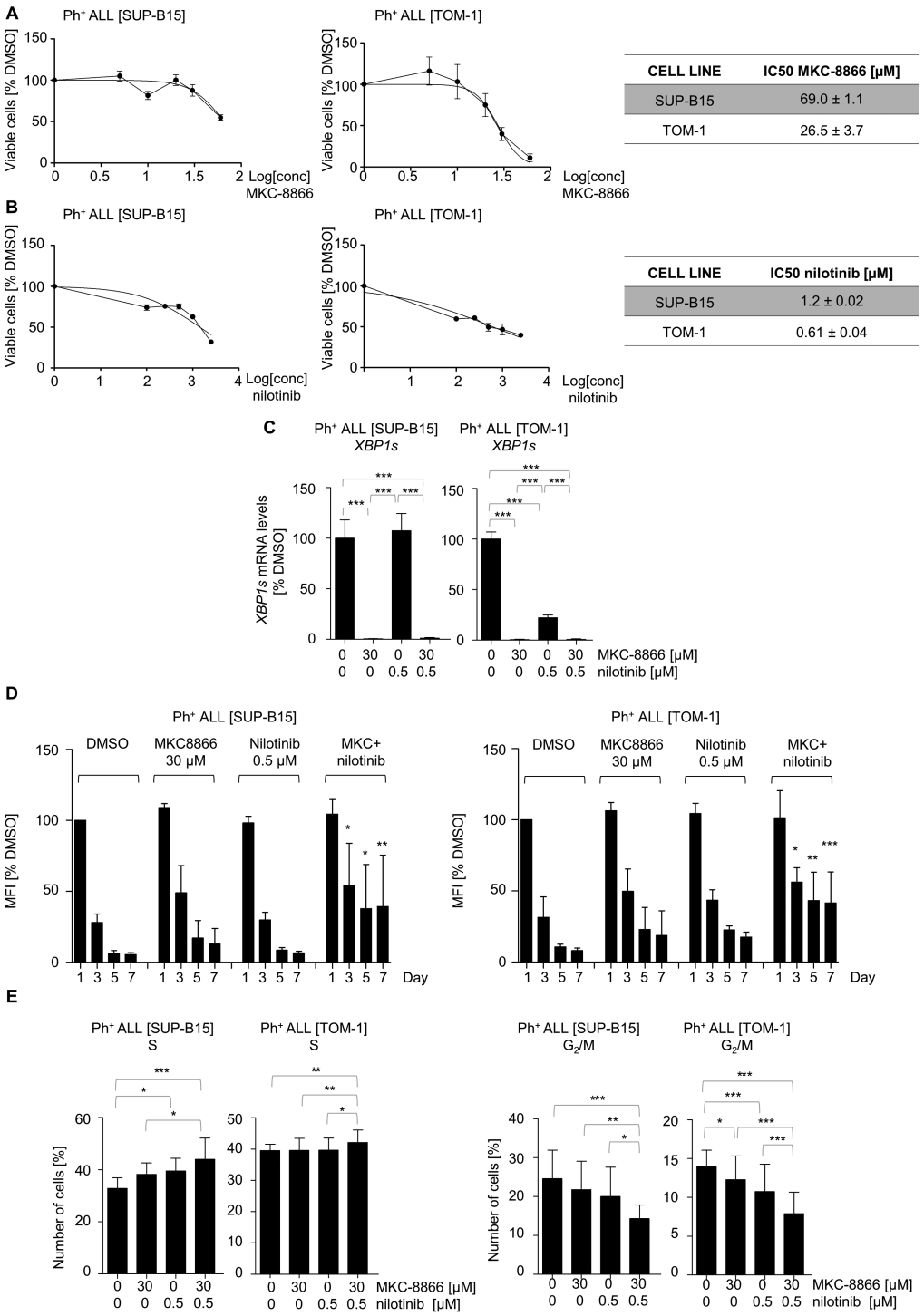

CELL LINE	IC50 MKC-8866 [μM]
SUP-B15	69.0 ± 1.1
TOM-1	26.5 ± 3.7

CELL LINE	IC50 nilotinib [μM]
SUP-B15	1.2 ± 0.02
TOM-1	0.61 ± 0.04

Figure 1. IRE1α RNase inhibitor MKC-8866 proves efficacy in high-risk ALL cells. **(A)** Dose-response curves obtained after treatment of Ph+ cell lines (SUP-B15, TOM-1) with DMSO and MKC-8866 5, 10, 20, 30 and 60 μM. The number of cells was determined by PI staining and quantitative measurement by FACS at day (d) 3. **(B)** Dose-response curves obtained after treatment of Ph+ cell lines (SUP-B15, TOM-1) with DMSO and nilotinib 0.1, 0.25, 0.5, 1 and 2.5 μM. The number of cells was determined by PI staining and quantitative measurement by FACS at d 3. The treatments shown in (A) and (B) were repeated in three independent experiments and three technical replicates were performed for each measurement. The non-linear regression was used to estimate the IC50 reported in the table on the right. **(C)** *XBP1s* mRNA levels were measured by quantitative real-time PCR in Ph+ ALL cell lines (SUP-B15, TOM-1) treated either with DMSO, MKC-8866 30 μM, nilotinib 0.5 μM and their combination for 16 h. *COX6b* was used as a housekeeping gene and results were normalized to DMSO values. One-way ANOVA was used as statistics. **(D)** SUB-B15 and TOM-1 cell lines were stained with CFSE 0.5 μM and then treated with DMSO, MKC-8866, nilotinib 0.5 μM or MKC-8866 30 μM + nilotinib 0.5 μM. At specific time points (d 1, d 3, d 5 and d 7) 5×10^5 cells were analyzed by FACS. The mean fluorescence intensity (MFI) for each condition normalized to DMSO d 1 values is shown. One-way ANOVA was used as statistics using DMSO d 3, d 5 and d 7 as control columns. **(E)** Ph+ cell lines were starved for 24 h (RPMI + 0% fetal bovine serum) and then released and treated with DMSO, MKC-8866 30 μM, nilotinib 0.5 μM and MKC-8866 30 μM + nilotinib 0.5 μM. The effect on cell cycle was assessed after 16 h. The analysis was performed staining the cells with PI. The graphs on the left report statistical analysis performed comparing the percentage of cells in S phase. The G2/M pool of cells is highlighted in the bar graphs on the right. Statistical analysis was performed via one-way ANOVA. All graphs depicted in this figure were obtained from the analysis of three independent experiments. Moreover, three technical replicates were performed for each measurement.

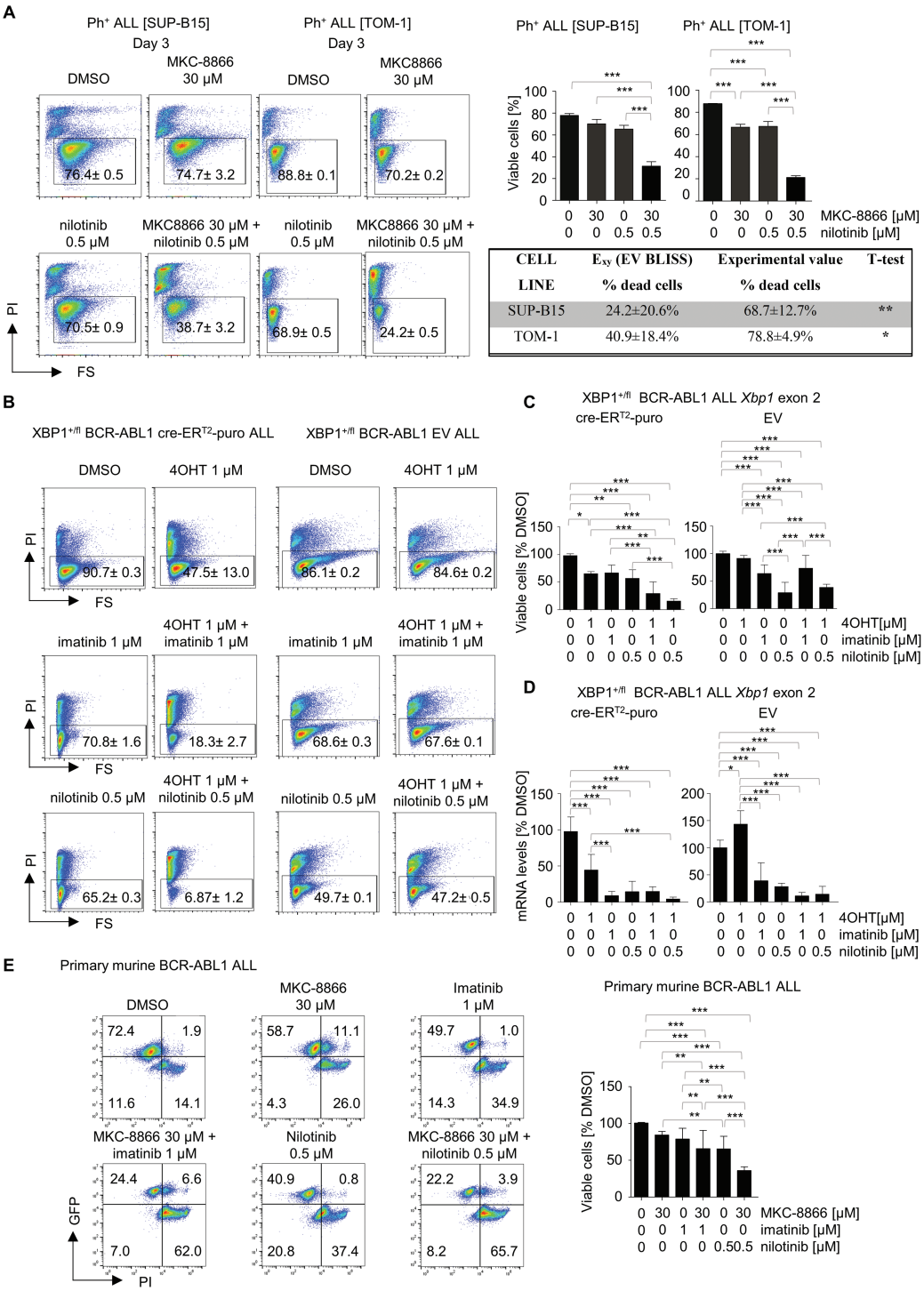

Figure 2. Treatment with MKC-8866 is synergistic with nilotinib in BCR-ABL1+ ALL and heterozygous deletion of *Xbp1* is sufficient to render BCR-ABL1+ ALL cells sensitive toward TKI treatment. **(A)** Ph+ ALL cell lines SUP-B15 and TOM-1 were treated with DMSO, MKC-8866 30 μM, nilotinib 0.5 μM or MKC-8866 30 μM + nilotinib 0.5 μM and the effect of viability was determined by PI staining at d 3. On the left, a representative experiment is shown and on the right percentages of viable cells are shown. One-way ANOVA was used as statistics. On the bottom right of this panel, Bliss formula calculations were performed to determine whether MKC-8866 in combination with nilotinib was synergistic. Results of three independent experiments were analyzed and t-test was applied for statistical analysis. **(B)** BCR-ABL1+ Xbp1+/fl ALL cells carrying cre or the empty vector were treated with DMSO, 4OHT 1 μM, imatinib 1 μM, nilotinib 0.5 μM or a combination of the two treatments (imatinib + 4OHT and nilotinib + 4OHT) and then viability was assessed by PI staining after 2 days. A representative experiment is shown in this panel. **(C)** Analysis of the three independent experiments of panel B. One-way ANOVA was used for statistical analysis. **(D)** BCR-ABL1+ Xbp1+/fl ALL cells transduced with cre or the empty vector were treated DMSO, 4OHT 1 μM, imatinib 1 μM, nilotinib 0.5 μM or combination of the two treatments (imatinib + 4OHT and nilotinib + 4OHT) for 24 h and *Xbp1* mRNA levels were assessed by quantitative real-time PCR amplifying exon 2, which resides between loxP sites of Xbp1 gene. *Hprt* was used as the housekeeping gene. One-way ANOVA was performed for statistical analysis. **(E)** Primary murine BCR-ABL1+ ALL cells were treated with DMSO, MKC-8866 30 μM, nilotinib 0.5 μM, imatinib 1 μM or the combination of the two treatments (imatinib + MKC-8866 and nilotinib + MKC-8866) and the effect of viability was determined by PI staining at d 3. On the left, a representative experiment is shown and on the right percentages of viable cells are depicted. One-way ANOVA was performed for statistical analysis. In this figure, all bar graphs were obtained analyzing three independent experiments and for each condition three technical replicates were performed, both in case of viability assays and the measurement of *Xbp1* mRNA levels.

(Figure 2D), whereas, with the human cell lines, only nilotinib exerted this effect (Figure 1C). Finally, we tested the effect of MKC-8866 in combination with either imatinib or nilotinib on murine primary BCR-ABL1+ ALL cells, showing again a significantly enhanced effect of the two classes of drugs compared with single treatments, similar to the observation with human cell lines (Figure 2E).

IRE1α and BCR-ABL1 signaling converge on multiple cell cycle regulators and apoptotic effectors

IRE1α signaling is known to positively regulate B-cell CLL/lymphoma 2 (BCL-2) family members (22). Therefore, we studied the effect of the combinational therapy with MKC-8866 and nilotinib on selected members of this family of proteins. Bcl-2-like protein 11 (also known as BIM), phorbol-12-myristate-13-acetate-induced protein 1 (PMAIP1, also known as NOXA) and proapoptotic Bcl-2-binding component 3 (also known as PUMA) are known executors of ER stress-mediated apoptosis (23–25). In our setup, BIM protein levels were upregulated with both single treatments and when the drugs were added simultaneously (Figure 3A and Supplementary Figure 4A). Moreover, *NOXA*, but not *PUMA*, mRNA expression levels were significantly increased upon dual therapy (Figure 3B and Supplementary Figure 3C). Other BCL-2 family members, such as BCL-2, Bcl-2-associated X protein (BAX), bcl-2 homologous antagonist/killer (BAK) and Bcl-2-associated agonist of cell death (BAD), have important roles in the cellular response to ER stress. Antiapoptotic BCL-2 is known to counteract apoptotic signal from the ER to the mitochondria. BAX and BAK are known to directly interact with IRE1α both in physiologic conditions and under proteostatic stress, being localized in the ER, as well as in the mitochondria (22). BAD is considered a candidate for transmitting the apoptotic signal from the ER to the mitochondria (26). However, these effectors were either not regulated by the treatments, such as *BAK*, *BAD* and *BAX* (Supplementary Figure 4B), or, in case of BCL-2, showed a minimal downregulation by both single and combination treatments (Supplementary Figure 4D). Their biological relevance is in this scenario, therefore, undetermined.

Lastly, given the fact that BCR-ABL1 is able to suppress tumor necrosis factor ligand superfamily member 10 (also known as TRAIL) mediated apoptosis (27,28), we analyzed whether the addition of MKC-8866 could alter *TRAIL* mRNA expression levels. This ligand was also strongly upregulated when MKC-8866 and nilotinib were used together (Figure 3C).

Next, we investigated whether cell cycle regulators are affected by treatment with MKC-8866 and nilotinib. The protein levels of cyclin-dependent kinase inhibitor 1B (also known as $p16^{INK4A}$), cyclin-dependent kinase inhibitor 1 (also known as $p21^{Waf1/Cip1}$) and cyclin-dependent kinase inhibitor 1B (also known as $p27^{Kip}$) were analyzed, given their role as major intersection points for several upstream pathways involved in the regulation of cell cycle (29) and, in our setup, the abundance of $p27^{Kip}$ was significantly increased upon combinational treatment in both cell lines (Figure 3D and Supplementary Figure 4E). This was also in good agreement with the fact that $p27^{Kip}$ was also significantly upregulated in murine primary BCR-ABL1+ ALL cells treated with the described combinations with both TKIs tested (Supplementary Figure 5). At this given time point, $p21^{Waf1/Cip1}$ showed a more intense expression in SUP-B15 upon dual treatment, whereas $p16^{INK4A}$ was more expressed in TOM-1 (Figure 3D), although not significantly different from the levels in nilotinib-treated cells. Finally, the inhibitory phosphorylation at Tyr15 of CDK2 was also found upregulated upon dual treatment when compared with DMSO (Figure 3E and Supplementary Figure 4F). Taken together, our data show that multiple inducers of apoptosis and negative regulators of cell cycle are affected by the dual treatment with MKC-8866 and nilotinib and, interestingly, the mechanism of action of both drugs seems to rely on the same effectors to induce cell death.

The dual treatment with MKC-8866 and nilotinib affects the expression of specific UPR proteins.

The three branches of the UPR are closely interconnected (30). We, therefore, analyzed the effect of our two agents on the ER stress sensor heat shock protein family A member 5 (*HSPA5*), as well as on *ATF6* and *PERK* pathways.

After dual treatment with MKC-8866 and nilotinib, *HSPA5* was downregulated by the drug combination (Supplementary Figure 6A), whereas *ATF6* levels were shown significantly upregulated in both cell lines when compared with its levels upon single treatment with either nilotinib or MKC-8866 or in untreated cells (Supplementary Figure 6B). PERK is known to inhibit protein synthesis by phosphorylating eukaryotic translation initiation factor 2 subunit alpha (eIF2α) on Ser51. In our experiments, phospho-eIF2α levels were upregulated upon single and dual treatment with MKC-8866 and nilotinib, with its levels upon combinational treatment being significantly different from the DMSO ones (Supplementary Figure 6C, top blots). On the other hand, IRE1α protein levels were left unchanged by the treatments (Supplementary Figure 6C, middle blots). The transcription factor DNA damage inducible transcript 3 (also known as CHOP) can regulate the transition of the UPR from its prosurvival phase to the proapoptotic one, when ER stress is prolonged (30,31). We, therefore, measured CHOP levels and we could observe its increase in all treated conditions when compared with DMSO levels (Supplementary Figure 6C, bottom blots). Overall, altering the levels of *XBP1s* with MKC-88666 alone or in combination with nilotinib had indirect effects on the other main executors of the UPR, which suggest the initiation of its proapoptotic response.

Phosphoproteome analysis reveals a differential regulation of p38α activation by MKC-8866 and nilotinib

To better understand the molecular basis of the observed synergism, a broad study of the proteome network was required and consecutively performed. Nilotinib is known to inhibit multiple kinases besides BCR-ABL1, such as ABL1, ABL2 and DDR1 (32). In addition, it is unknown whether the pharmacological inhibition of the RNase domain of IRE1α could have an impact on the phosphoproteome since the drug is not directly affecting the IRE1α kinase domain. For these reasons, both the SUP-B15 and the TOM-1 cell lines were treated with DMSO, MKC-8866, nilotinib and the combination of these two drugs for 16 h and then subjected to phosphoproteomic analysis.

First, this analysis showed that the combined effect of MKC-8866 and nilotinib caused a substantial downregulation of five retinoblastoma (RB1) inhibitory phosphorylation sites (S780, S788, S795, S807 and S811) and an increased abundance of cyclin-dependent kinases 2, 4 and/or 6 (CDK2/CDK4/CDK6) inhibitory phosphorylations T14 and Y15 (Supplementary Table 3) in line with the results shown in Figure 3E and Supplementary Figure 4F. Phospho-RB1 (Ser807/811) levels were measured via western blot and we could confirm its downregulation in both

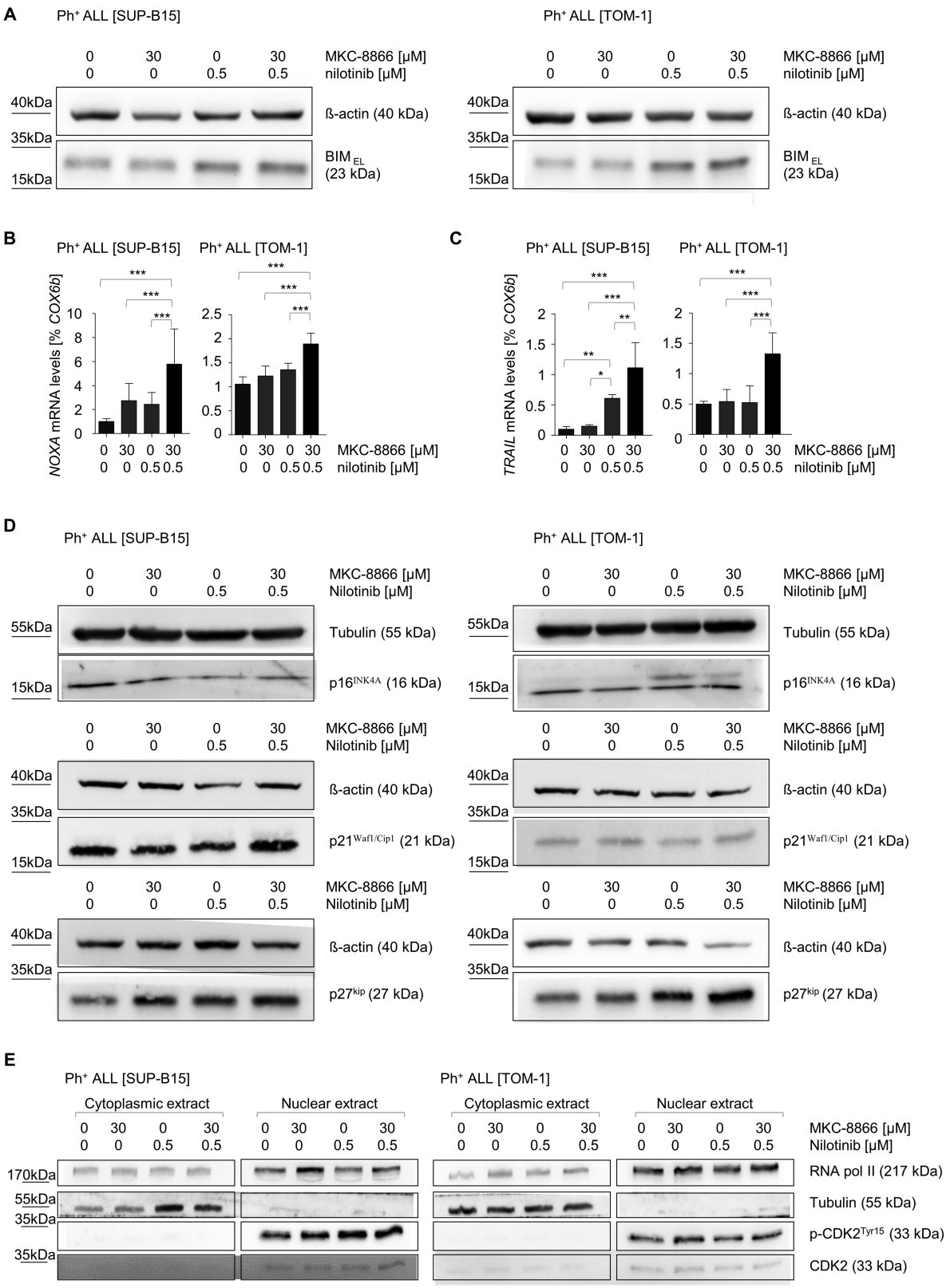

Figure 3. Dual treatment with MKC-8866 and nilotinib modulates the expression of specific apoptotic effectors and cell cycle regulators. **(A)** Western-blot analysis of BIM in SUP-B15 and TOM-1 treated for 16 h with DMSO, MKC-8866 30 μM, nilotinib 0.5 μM, MKC-8866 30 μM + nilotinib 0.5 μM. β-actin expression was used as loading control. *NOXA* **(B)** and *TRAIL* **(C)** mRNA levels were measured by quantitative real-time PCR in Ph+ ALL cell lines (SUP-B15, TOM-1) treated with DMSO, MKC-8866 30 μM, nilotinib 0.5 μM, MKC-8866 30 μM + nilotinib 0.5 μM for 16 h. *COX6b* was used as the housekeeping gene. Bar graphs were obtained by analyzing three independent experiments with three technical replicates for each condition. One-way ANOVA was performed for statistical analysis. **(D)** Western-blot analysis of $p16^{INK4A}$, $p21^{Waf1/Cip1}$ and $p27^{Kip}$ in SUP-B15 and TOM-1 treated for 16 h with DMSO, MKC-8866 30 μM, nilotinib 0.5 μM, MKC-8866 30 μM + nilotinib 0.5 μM. β-actin or tubulin expression were used as a loading control. **(E)** SUP-B15 and TOM-1 were treated for 16 h with DMSO, MKC-8866 30 μM, nilotinib 0.5 μM, MKC-8866 30 μM + nilotinib 0.5 μM. Protein lysates of the cytoplasmic and nuclear extract were obtained and p-$CDK2^{tyr15}$ expression was analyzed. Total CDK2 levels, as well as RNA pol II and tubulin levels, were used as controls. Densitometry analyses for experiments in (A), (D) and (E) are shown in Supplementary Figure 4.

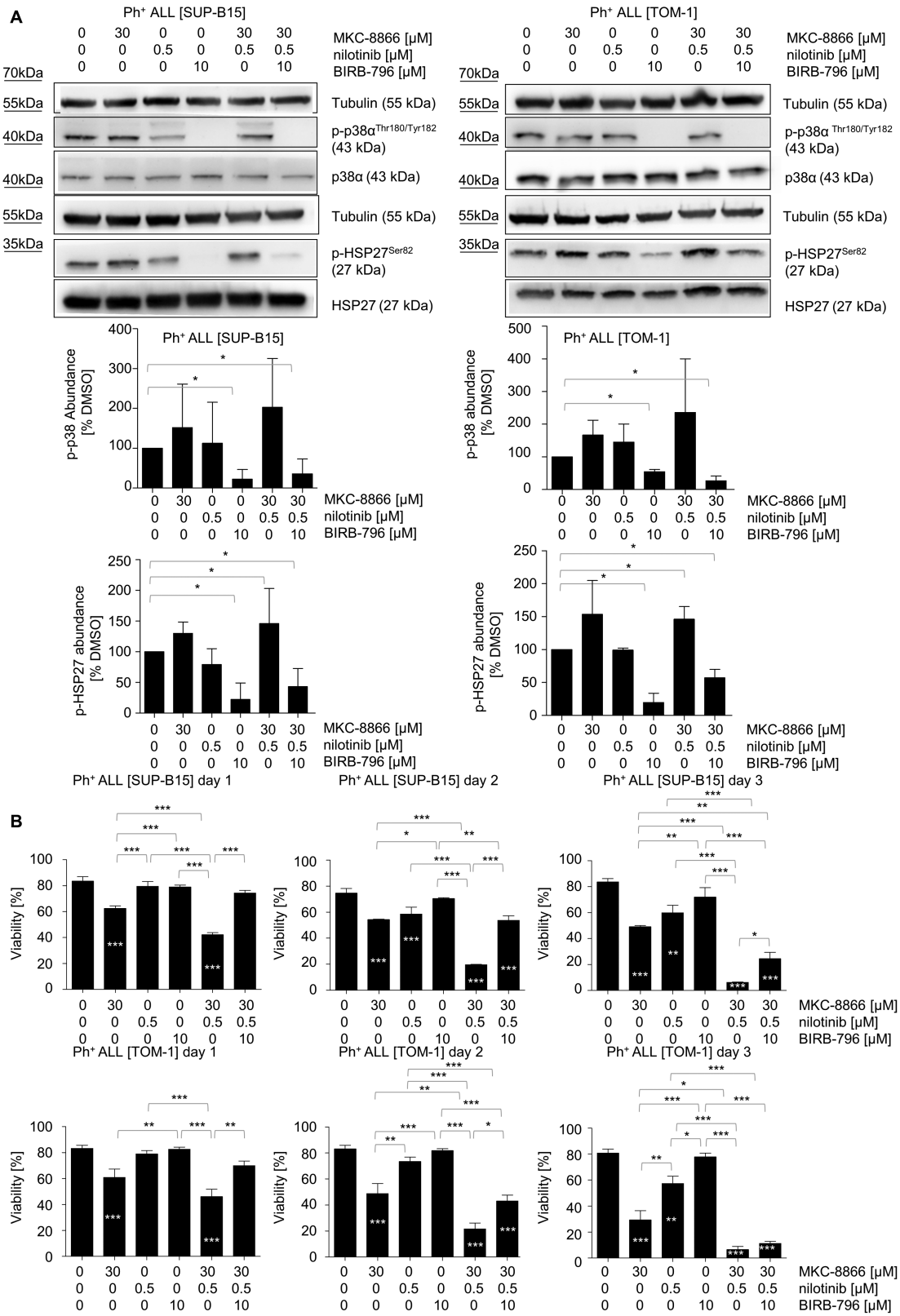

Figure 4. Inhibition of p38 MAPK using the inhibitor BIRB-796 reverts the synergistic effect of MKC-8866 and nilotinib. **(A)** Western-blot analysis of phospho-p38$^{Thr180/Tyr182}$, p38, phospho-HSP27^{Ser82} and HSP27 proteins expression in SUP-B15 and TOM-1 treated for 16 h with DMSO, MKC-8866 30 μM, nilotinib 0.5 μM, BIRB-796 10 μM, MKC-8866 30 μM + nilotinib 0.5 μM and MKC-8866 30 μM + nilotinib 0.5μM + BIRB-796 10μM. Tubulin expression was used as a loading control. The bar graphs under the blots show the densitometry analysis performed for phospho-p38 (top graphs) and phospho-HSP27 (bottom graphs) using ImageJ® software. Three independent blots were analyzed and the reported statistical significance was calculated with a one-sample *t*-test. **(B)** Ph+ ALL cell lines SUP-B15 and TOM-1 were treated with DMSO, MKC-8866 30 μM, BIRB-796 10 μM, MKC-8866 30 μM + nilotinib 0.5 μM and MKC-8866 30 μM + nilotinib 0.5 μM + BIRB-796 10 μM and the effect of viability was determined by PI staining at different time points (d 1, d 2 and d 3). The graphs were obtained by analyzing three independent experiments and three technical replicates were performed for each condition. One-way ANOVA was used as statistics. White stars highlight statistical differences with the DMSO column.

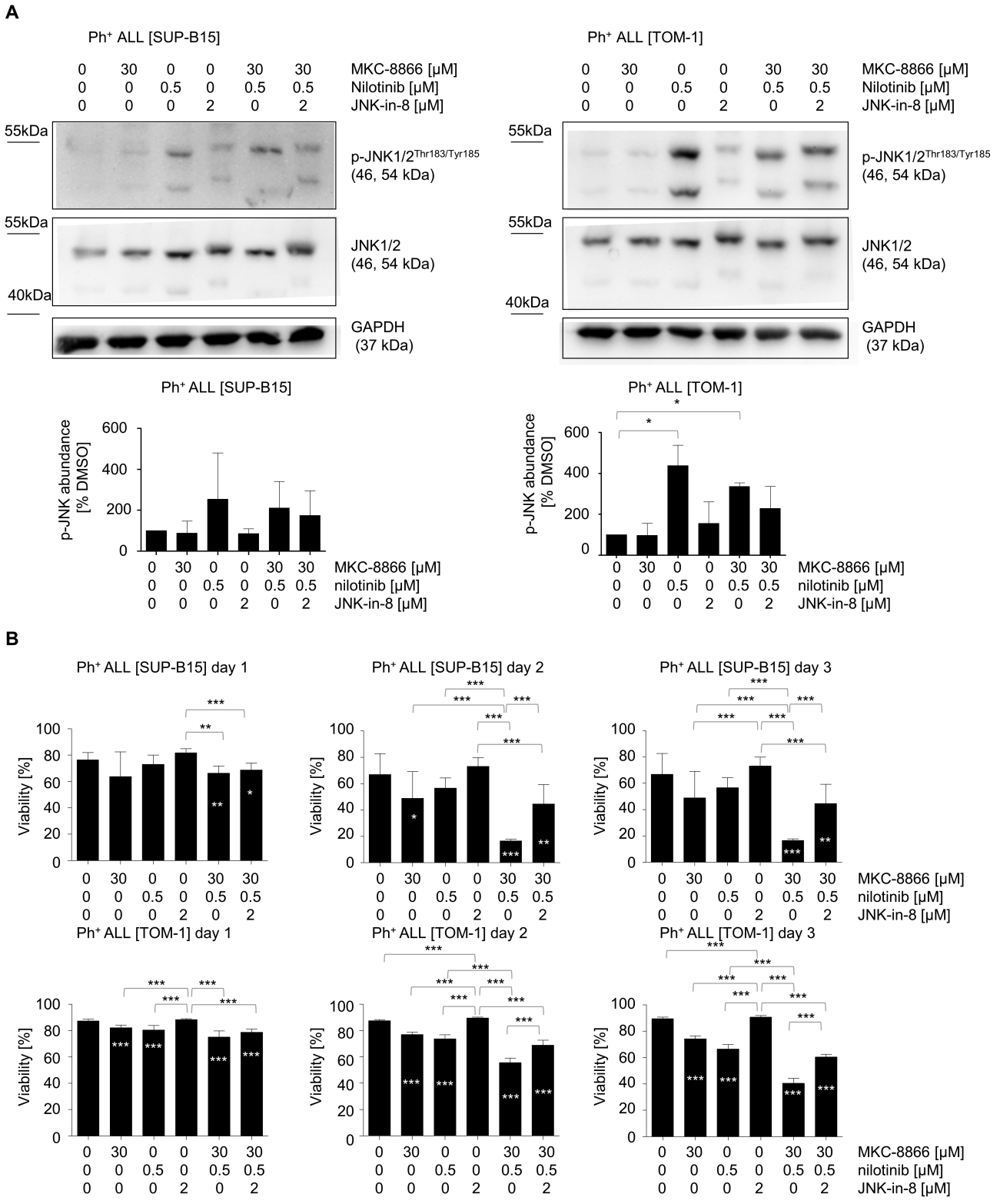

Figure 5. Inhibition of JNK using the inhibitor JNK-in-8 reverts the synergistic effect of MKC-8866 and nilotinib. **(A)** Western-blot analysis of phospho-JNK1/2$^{Thr183/Tyr185}$, JNK1/2 proteins expression in SUP-B15 and TOM-1 treated for 16 h with DMSO, MKC-8866 30 μM, nilotinib 0.5 μM, JNK-in-8 2 μM, MKC-8866 30 μM + nilotinib 0.5 μM and MKC-8866 30 μM + nilotinib 0.5μM + JNK-in-8 2 μM. Tubulin expression is used as loading control. The bar graphs under the blots show the densitometry analysis performed for phospho-JNK1/2 using ImageJ® software. Three independent blots were analyzed and the reported statistical significance was calculated with one-sample *t*-test. **(B)** Ph+ ALL cell lines SUP-B15 and TOM-1 were treated with DMSO, MKC-8866 30 μM, nilotinib 0.5 μM, JNK-in-8 2 μM, MKC-8866 30 μM + nilotinib 0.5 μM and MKC-8866 30 μM + nilotinib 0.5μM + JNK-in-8 2 μM and the effect of viability was determined by PI staining at different time points (d 1, d 2 and d 3). The graphs were obtained by analyzing three independent experiments and three technical replicates were performed for each measurement. One-way ANOVA was performed for statistical analysis. White stars highlight statistical differences in comparison to the DMSO column.

cell lines when MKC-8866 is used in combination with nilotinib (Supplementary Figure 6D).

We successively utilized publicly available databases in order to predict the candidate targeting kinases for all the phosphosites that were altered by the different treatments (log fold change >|1| when compared with DMSO). Several phosphorylation sites targeted by p38α (MAPK14) and its two main downstream kinases MAPK-activated protein kinase 2 and 3 were found increased upon IRE1 inhibition alone or, more importantly, in combination with the TKI (Supplementary Table 5). Given the fact that most of the substrates found regulated by the treatments are targeted by more than one kinase, we ought to validate via western blot the modulation of p38 MAPK.

We, therefore, analyzed its activating phosphorylation on Thr180/Tyr182 and the involvement of its downstream target heat shock protein beta-1 (also known as HSP27), measuring the levels of one of the p38-dependent phosphorylation sites reported, Ser82 (Figure 4A). After 16 h of treatment, MKC-8866 alone or in combination with nilotinib caused a significant upregulation of phospho-HSP27 when compared with DMSO levels, whereas the upregulation of phospho-p38 itself was marginal. On the other hand, we could observe a significant upregulation of phospho-p38 in the SUP-B15 cells after 6 h of treatment with MKC-8866 alone or combined with nilotinib (Supplementary Figure 7). To test whether the activation of p38 MAPK had an actual role in the synergistic effect of MKC-8866 and nilotinib combined, we analyzed the consequences of its pharmacological inhibition during the combinational treatment.

Interestingly, pharmacological inhibition of p38 MAPK with the small molecule BIRB-796 could hinder the combined effect of MKC-8866 and nilotinib on human leukemia cell viability, restoring the percentage of living cells to the levels of the single treatment, after 24 or 48 h of treatment, while the rescue was only partial after 72 h (Figure 4B). In addition, the effect of dual inhibition of BCR-ABL1 and p38 MAPK with nilotinib and BIRB-796, as well as of IRE1α and p38 MAPK, is not significantly different from the one exerted by nilotinib or MKC-8866 alone, respectively (Supplementary Figure 8A). Similarly to p38 MAPK, c-Jun N-terminal kinase 1/2 (JNK1/2) are important kinases involved in the XBP1-independent response to ER stress by IRE1α (6). Given its similar role to p38 MAPK in response to ER stress, we extended our investigation toward JNK1/2 as well, although the phosphoproteome analysis did not show a consistent role in our combinational treatment. Nevertheless, we could show that JNK1/2 were phosphorylated on Thr183/Tyr185 when cells were treated with the combination of MKC-8866 and nilotinib. Interestingly, the main activator of JNK1/2 resulted to be nilotinib since phospho-JNK1/2 were upregulated upon single TKI inhibition, whereas IRE1α inhibition did not modulate their levels (Figure 5A). Next, we tested again the consequences of JNK1/2 inhibition, using the inhibitor JNK-in-8, during the combinational treatment. JNK-in-8 does not modify the phosphorylation state of JNK1/2, but it causes a reduction in the electrophoretic mobility of JNK1/2 proteins, probably caused by its covalent modification (Figure 5A) (33). Similarly to what was observed with p38α inhibition, the synergistic effect of MKC-8866 and nilotinib was significantly impaired by the inhibition of JNK1/2, underlining the important role of this kinase in the cytotoxic effect observed (Figure 5B), even though the activation of JNK/2 might not be dependent on IRE1α inhibition, but mainly be caused by nilotinib. In line with this finding, in Supplementary Figure 8B, we could show that nilotinib, in combination with JNK-in-8, is less effective at least in TOM-1, although not drastically. Taken together, these results suggest that the activation of p38 MAPK, mostly due to the activity of MKC-8866 and of JNK1/2, as an effect of nilotinib treatment, seem to be pivotal for the success of the combination of BCR-ABL1 and IRE1α pharmacological inhibition.

Discussion

Our current study provides additional evidence for the importance of the IRE1α signaling in Ph$^+$ ALL and points to a relevant therapeutic potential of the clinical candidate MKC-8866 in this setting. Our studies indicate that targeting IRE1α signaling by MKC-8866 leads (i) to reduced proliferation of human ALL cells and (ii) is synergistic with TKIs (i.e. imatinib and nilotinib) when used for the treatment of this high-risk subset of ALL. Furthermore, these pharmacological effects are recapitulated in a genetic conditional heterozygous murine Ph$^+$ ALL-like model and seem to be mostly mediated via signaling through the p38 MAPK and JNK pathways.

While previous IRE1α inhibitors, including STF-083010 or A106, were used to provide early proof of principle, they were not suitable for *in vivo* application and potential later clinical testing due to their unfavorable pharmacodynamics and toxicity profile (34). In contrast, the compound MKC-8866 has been significantly improved, rendering it a suitable candidate for potential further clinical development (18,19).

With MKC-8866 monotherapy already providing a strong basis for its relevance as a potential therapeutic agent, we aimed to further characterize if it could also act synergistically with treatment options already established for the treatment of Ph$^+$ ALL, such as BCR-ABL1 TKIs. Our findings confirmed synergism with nilotinib, one clinically established agent for the treatment of Ph$^+$ ALL.

The major effects of combined treatment with MKC-8866 and nilotinib were proliferation arrest and finally cell death. Induction of apoptosis was confirmed by the upregulation of the proapoptotic markers BIM and *NOXA*. These results point to the likelihood that the induction of such proapoptotic effectors might be due to sustained and unresolved ER stress. Both BIM and NOXA are known mediators of apoptosis under ER stress (23–25) and their upregulation in this context can be at least in part mediated by CHOP (23,24), which has been found to be upregulated upon dual treatment with MKC-8866 and nilotinib as well. Moreover, the induction of CHOP can be mediated by both the PERK and ATF6 pathways of UPR (35), which are both found activated in our combinational treatment. Remarkably, even *HSPA5*, which has antiapoptotic properties in pre-B-cell precursors (36), was found significantly less abundant upon combined treatment, further underscoring the potent effect of our proposed treatment toward major linchpins of pre-B-ALL survival.

It is interesting to note that, *TRAIL*, a proapoptotic ligand belonging to the TNF family was observed as being more abundant upon dual treatment. How this effect is precisely exerted has not been elucidated but, interestingly, the promoter of *TRAIL*, as well as the ones of *NOXA*, *BIM*, p21$^{Waf1/Cip1}$ and p27^{Kip} are the target of Forkhead box protein O1 and O3 (FoxO1/3) activity (37), which, in turn, can be phosphorylated in B-ALL by stress kinases, such as JNK or p38 MAPK, in response to different agents, such as doxorubicin or dexamethasone, thus promoting its nuclear localization and activation (38,39). Whether the activation of p38α and/or JNK1 upon combined treatment with MKC-8866 and nilotinib has a role in *TRAIL* upregulation has yet to be validated.

The combination therapy was also able to induce cell cycle alterations, supposedly arresting the cells during either G1 or S

phase and impeding the completion of the cell cycle. In fact, our data suggests that CDK2/CDK4/CDK6 might be inhibited, thus leading to a consequent hypophosphorylation of RB1. This is probably due to the increased levels of cell cycle regulators, such as $p16^{INK4A}$, $p21^{Waf1/Cip1}$ and $p27^{Kip}$, in both cell lines, although only the latter was the most consistently upregulated marker.

By employing a genetic model of BCR-ABL1$^+$ ALL, we excluded off-target effects caused by the combination of MKC-8866 and nilotinib. Heterozygous deletion of *Xbp1* sensitized the *Xbp1*$^{+/fl}$ BCR-ABL1$^+$ ALL cells toward TKI-induced cell death, again underlining the crucial role of XBP1 activity in this malignant setting. The use of conditional knockout mice for *Xbp1* instead of IRE1α allowed us to interrupt only Xbp1 signaling, while kinase domain-related signaling remained intact, particularly the activation of JNK and p38 MAPK kinases, which are thought to initiate IRE1α-mediated apoptosis (6).

Finally, we wanted to elucidate the molecular mechanism at the basis of this synergism. We performed a phosphoproteome analysis, which suggested an induction of the p38α kinase axis. In response to prolonged ER stress, IRE1α is known to bind specific cytosolic partners that participate in the activation of an XBP1-independent response to ER stress. Tumor necrosis factor receptor-associated factor 2 is in fact recruited by IRE1α, and this event eventually leads to the activation of JNK or p38 MAPK (6,40). We, therefore, investigated the role of p38 MAPK during simultaneous inhibition of IRE1α and BCR-ABL1 in Ph$^+$ ALL by inhibiting it with BIRB-796. We observed that, without the activity of p38 MAPK, cell death induced by dual treatment was significantly hindered, so that the success of our proposed treatment seems to be dependent at least in part on the activation of p38 MAPK. This enhanced activity was shown rather by a constant increased phosphorylation of its downstream target HSP27 on Ser82 after 6 and 16 h of treatment than by the phosphorylation of p38 MAPK itself. Nevertheless, we could also observe a clear upregulation of phospho-p38 in SUP-B15 after 6 h of treatment. We hypothesize to have a similar upregulation in TOM-1 cells at an earlier time point, suggesting a slightly different time of reaction of this stress kinase to the treatment. This hypothesis is supported by the fact that phospho-HSP27 is already more abundant after 6 h in this cell line.

Overall, this increased activity of p38 MAPK was present both in cells treated with MKC-8866 alone or in combination, strongly suggesting that this process could rely at least in part on the activity of the IRE1α kinase domain. MKC-8866, by blocking IRE1α prosurvival pathway governed by XBP1, can cause a prolonged ER stress that activates the proapoptotic functions of the IRE1 kinase domain, culminating in a potent cytotoxic effect.

As mentioned above, another important stress kinase activated by IRE1α is JNK (40). We evaluated the importance of this protein following the same method used for p38 MAPK and observed similar results: inhibiting JNK1/2 significantly impairs the efficacy of MKC-8866 and nilotinib together. However, the involvement of JNK1/2 seems to be due to the signaling of nilotinib and not as expected by IRE1α inhibition. Of note, the analysis of the phosphoproteomic data performed to predict the kinases involved in the combinational treatment did not show a clear regulation of JNK1, evidencing three to six of its targets with a reduced phosphorylation after the administration of single treatments. This is due to the fact that most of the substrates can be phosphorylated on a specific site by multiple kinases, ultimately making necessary to perform validations of the results obtained with low-throughput techniques.

In conclusion, this body of evidence may successfully address a gap in the therapeutic armamentarium against this aggressive leukemia, especially in elderly patients not eligible for allogeneic stem cell transplantation. Pending is an *in vivo* validation of such proposed treatment; this may, hence, provide a novel targeted therapeutic approach for this subset of patients with particularly dismal prognosis.

Supplementary material

Supplementary data are available at *Carcinogenesis* online.

Supplementary Figure 1: CFSE assay of high-risk ALL cells treated with TKI in combination with MKC-8866

(A) Representative experiment of the analysis shown in Figure 1D. **(B)** Representative experiment of the analysis shown in Figure 1D but using imatinib 10 μM instead of nilotinib 0.5 μM. The analysis of this experiment is shown in Supplementary Figure 2B. **(C)** FSC and SSC plots of a representative CFSE experiment performed with SUP-B15 (left) and TOM-1 (right).

Supplementary Figure 2: Treatment with MKC-8866 is synergistic with imatinib in Ph$^+$ ALL. (A) Ph$^+$ ALL cell lines SUP-B15 and TOM-1 were treated with DMSO, MKC-8866 30 μM, imatinib 10 μM or MKC-8866 30 μM + imatinib 10 μM and the effect of viability was determined by PI staining at d 3. On the left a representative experiment is shown and on the right percentages of viable cells are shown. This graph was obtained analysing three independent experiments. 1-way ANOVA was used as statistics. **(B)** SUB-B15 and TOM-1 cell lines were stained with CFSE 0.5 μM and then treated with DMSO, MKC-8866, imatinib 10 μM or MKC-8866 30 μM + imatinib 10 μM. At specific timepoints (d 0, d 1, d 3, d 5 and d 7) 5×10^5 cells were analyzed by FACS. The Mean Fluorescence Intensity (MFI) for each condition, normalized to DMSO d 1 values is shown. The graphs were obtained from the analysis of three independent experiments. 1-way ANOVA was performed for statistical analysis, using DMSO at d 3, d 5 and d 7 as control columns. **(C)** *XBP1s* mRNA levels were measured by qRT-PCR in Ph$^+$ ALL cell lines (SUP-B15, TOM-1) treated either with DMSO, MKC-8866 30 μM, imatinib 10 μM and their combination for 16 h. *COX6b* was used as a housekeeping gene and results were normalized to DMSO values. The treatment was repeated in three independent experiments and 3 technical replicates are performed for each condition. 1-way ANOVA was performed for statistical analysis.

Supplementary Figure 3: No effect of MKC-8866 and nilotinib on non Ph+ ALL cell lines REH and SEM.

Non Ph$^+$ ALL ETV-RUNX1$^+$ cell line REH and MLL-AF4$^+$ cell line SEM were treated with DMSO, MKC-8866 30 μM, nilotinib 0.5 μM and their combination and their viability was assessed at d 1, d 2 and d 3 using methylene blue assay. No statistical differences between the treatment groups were observed using a 2-way ANOVA test.

Supplementary Figure 4: Dual treatment with MKC-8866 and nilotinib regulates the expression of specific apoptotic and cell cycle effectors. (A) Densitometry analysis performed for BIM in Ph$^+$ ALL cell lines (SUP-B15, TOM-1) treated with DMSO, MKC-8866 30 μM, nilotinib 0.5 μM, MKC-8866 30 μM + nilotinib 0.5 μM for 16 h. *BAK, BAD, BAX* (**B**) and *PUMA* (**C**) mRNA levels were measured by q-RT-PCR. *COX6b* has been used as housekeeping gene. Bar graphs were obtained analyzing three independent experiments with three technical replicates for each condition. **(D)** BCL-2 protein levels. On the top representative blots for BCL-2 in SUP-B15 and TOM1 are shown. On the bottom of the panel a respective densitometry analysis performed is shown. **(E)** Densitometry analysis performed for $p16^{INK4A}$, $p21^{Waf1/Cip1}$, $p27^{Kip}$ in Ph$^+$ ALL cell lines. **(F)** Densitometry analysis performed for p-CDK2 in Ph$^+$ ALL cell lines. Each densitometry in this figure

was obtained after the analysis of three independent blots using ImageJ software. The reported statistical significance was calculated by applying a 1-way ANOVA.

Supplementary Figure 5: Up-regulation of p27 after treatment with MKC-8866 in combination with TKIs in mouse primary BCR-ABL1 ALL cells. (A) Western-blot analysis of $p27^{Kip}$ protein expression in BCR-ABL1^{+} Xbp1$^{+/fl}$ ALL cells treated for 16 h with DMSO, MKC-8866 30 μM, imatinib 10 μM, nilotinib 0.5 μM, MKC-8866 30 μM + imatinib 10 μM and MKC-8866 30 μM + nilotinib 0.5 μM. Tubulin expression was used as loading control. The bar graphs on the right show the densitometry analysis performed for $p27^{Kip}$ (left) using ImageJ® software. Three independent blots were analyzed and the reported statistical significance was calculated with one sample t-test.

Supplementary Figure 6: Expression levels of main UPR effectors after treatment of Ph^{+} ALL cell lines with MKC-8866, nilotinib and their combination. *HSPA5* **(A)** and *ATF6* **(B)** mRNA levels were measured by qRT-PCR in Ph^{+} ALL cell lines (SUP-B15, TOM-1) treated either with DMSO, MKC-8866 30 μM, nilotinib 0.5 μM and their combination for 16 h. *COX6b* was used as the housekeeping gene and results were normalized to DMSO values. 1-way ANOVA was used as statistics. **(C)** phospho- eIF2α^{Ser51} (top blots) and IRE1α (bottom blots) protein levels were measured in SUP-B15 and TOM-1. The densitometry analysis for phospho-eIF2α^{Ser51} is shown on the right of this panel. One sample t-test was used as statistics. **(D)** phospho-RB1$^{Ser807/811}$ protein levels were measured in SUP-B15 and TOM-1 treated with DMSO, MKC-8866 30 μM, nilotinib 0.5 μM, MKC-8866 30 μM + nilotinib 0.5 μM. The densitometry analysis is shown on the right for both cell lines. A one sample t-test was used to test for statistical significance. In this figure, each bar graph was obtained after the analysis of three independent experiments, as well as the densitometries were performed analysing three independent blots. Moreover, three technical replicates for data obtained with via qRT-PCR were performed for each condition.

Supplementary Figure 7: After 6 hours of treatment with MKC-8866, p38 MAPK is more phosphorylated in SUP-B15 cells. Western-blot analysis of phospho-p38$^{Thr180/Tyr182}$, p38, phospho-HSP27^{Ser82} and HSP27 proteins expression in SUP-B15 and TOM-1 treated for 6 h with DMSO, MKC-8866 30 μM, nilotinib 0.5 μM, BIRB-796 10 μM, MKC-8866 30 μM + nilotinib 0.5 μM and MKC-8866 30 μM + nilotinib 0.5μM + BIRB-796 10μM. Tubulin expression was used as a loading control.

Supplementary Figure 8: p38 MAPK and JNK inhibition in Ph^{+} ALL. (A) Treatment of Ph^{+} ALL cell lines SUP-B15 and TOM-1 with DMSO, MKC-8866 30 μM, BIRB-796 10 μM, MKC-8866 30 μM + BIRB-796 10 μM and BIRB-796 10 μM + nilotinib 0.5 μM was performed for 3 days. A representative experiment is shown for both cell lines. **(B)** Treatment of Ph^{+} ALL cell lines SUP-B15 and TOM-1 with DMSO, MKC-8866 30 μM, JNK-in-8 2 μM, MKC-8866 30 μM + JNK-in-8 2 μM and JNK-in-8 2 μM + nilotinib 0.5 μM was performed for 3 days. A representative experiment is shown for both cell lines. On the bottom of this panel bar graphs obtained after the analysis of three independent experiment per cell line are shown. 1-way ANOVA was performed for statistical analysis

Acknowledgements

We would like to thank Laurie H Glimcher (Weill Cornell College of Medicine, New York, NY) for *Xbp1*$^{fl/fl}$ mice. Finally yet importantly, we would like to thank Kema Marlen Schröder for technical support.

Funding

This work is supported by funding from the Ernst Jung Foundation, Rheinisch-Westfälische Technische Hochschule Aachen (RWTH) START and RWTH START UP to B.K.M.; RWTH Habilitationsfoerderung to I.A., German Cancer Aid (Deutsche Krebshilfe, grant number 70111714) to B.K.M./I.A., Science Foundation Ireland grant co-funded under the European Regional Development Fund (grant number 13/RC/2073, EU H2020 MSCA ITN-675448 (TRAINERS) and EU H2020 MSCA RISE-734749 (INSPIRED) to Af.S.).

Conflict of Interest Statement: T.H.B.: consultancy (Novartis, Pfizer, Janssen, Merck, Takeda), research funding (Novartis, Pfizer). J.B.P. was an employee of Mannkind Corp. and is currently employed by Fosun Orinove PharmaTech, Inc. B.K.M., and I.A. received research funding from Takeda and Novartis. All other authors have declared no competing interests.

Authors' contributions

M.V. designed and performed experiments, analyzed the results and wrote the manuscript. C.P. performed mass spectrometry experiments and analyzed the results. M.S., A.S., J.B.P., Af.S. and T.H.B. supported analysis. B.K.M. and I.A. conceptually designed the study and I.A. was a major contributor in writing the manuscript. All authors discussed the results and commented on the manuscript. All authors read and approved the final manuscript.

Ethics statement

All experiments involving the use of animals were conducted according to the German Animal Protection legislation. The animal protocol number AZ84-02.04.2015.A328 was approved by the local authorities of North Rhine-Westphalia.

References

1. Díaz-Villanueva, J.F. *et al.* (2015) Protein folding and mechanisms of proteostasis. *Int. J. Mol. Sci.,* 16, 17193–17230.
2. Chevet, E. *et al.* (2015) Endoplasmic reticulum stress-activated cell reprogramming in oncogenesis. *Cancer Discov.,* 5, 586–597.
3. Kharabi Masouleh, B. *et al.* (2015) Drugging the unfolded protein response in acute leukemias. *J. Hematol. Oncol.,* 8, 87.
4. Bertolotti, A. *et al.* (2000) Dynamic interaction of BiP and ER stress transducers in the unfolded-protein response. *Nat. Cell Biol.,* 2, 326–332.
5. Uemura, A. *et al.* (2009) Unconventional splicing of XBP1 mRNA occurs in the cytoplasm during the mammalian unfolded protein response. *J. Cell Sci.,* 122(Pt 16), 2877–2886.
6. Darling, N.J. *et al.* (2014) The role of MAPK signalling pathways in the response to endoplasmic reticulum stress. *Biochim. Biophys. Acta,* 1843, 2150–2163.
7. Li, B. *et al.* (2011) Differences in endoplasmic reticulum stress signalling kinetics determine cell survival outcome through activation of MKP-1. *Cell. Signal.,* 23, 35–45.
8. Papandreou, I. *et al.* (2011) Identification of an Ire1alpha endonuclease specific inhibitor with cytotoxic activity against human multiple myeloma. *Blood,* 117, 1311–1314.
9. Tang, C.H. *et al.* (2014) Inhibition of ER stress-associated IRE-1/XBP-1 pathway reduces leukemic cell survival. *J. Clin. Invest.,* 124, 2585–2598.
10. Ming, J. *et al.* (2015) A novel chemical, STF-083010, reverses tamoxifen-related drug resistance in breast cancer by inhibiting IRE1/XBP1. *Oncotarget,* 6, 40692–40703.
11. Chien, W. *et al.* (2014) Selective inhibition of unfolded protein response induces apoptosis in pancreatic cancer cells. *Oncotarget,* 5, 4881–4894.
12. Sun, H. *et al.* (2016) Inhibition of IRE1α-driven pro-survival pathways is a promising therapeutic application in acute myeloid leukemia. *Oncotarget,* 7, 18736–18749.

13. Kharabi Masouleh, B. *et al.* (2014) Mechanistic rationale for targeting the unfolded protein response in pre-B acute lymphoblastic leukemia. *Proc. Natl. Acad. Sci. USA,* 111, E2219–E2228.
14. Hunger, S.P. *et al.* (2015) Redefining ALL classification: toward detecting high-risk ALL and implementing precision medicine. *Blood,* 125, 3977–3987.
15. Castro, F. *et al.* (2013) High-throughput SNP-based authentication of human cell lines. *Int. J. Cancer,* 132, 308–314.
16. Vizcaíno, J.A. *et al.* (2016) 2016 update of the PRIDE database and its related tools. *Nucleic Acids Res.,* 44, 11033.
17. Greco, W.R. *et al.* (1995) The search for synergy: a critical review from a response surface perspective. *Pharmacol. Rev.,* 47, 331–385.
18. Logue, S.E. *et al.* (2018) Inhibition of IRE1 RNase activity modulates the tumor cell secretome and enhances response to chemotherapy. *Nat. Commun.,* 9, 3267.
19. Zhao, N. *et al.* (2018) Pharmacological targeting of MYC-regulated IRE1/XBP1 pathway suppresses MYC-driven breast cancer. *J. Clin. Invest.,* 128, 1283–1299.
20. Tallarida, R.J. (2011) Quantitative methods for assessing drug synergism. *Genes Cancer,* 2, 1003–1008.
21. Westbrook, C.A. *et al.* (1992) Clinical significance of the BCR-ABL fusion gene in adult acute lymphoblastic leukemia: a cancer and leukemia group B study (8762). *Blood,* 80, 2983–2990.
22. Hetz, C. *et al.* (2006) Proapoptotic BAX and BAK modulate the unfolded protein response by a direct interaction with IRE1alpha. *Science,* 312, 572–576.
23. Puthalakath, H. *et al.* (2007) ER stress triggers apoptosis by activating BH3-only protein Bim. *Cell,* 129, 1337–1349.
24. Li, J. *et al.* (2006) Endoplasmic reticulum stress-induced apoptosis: multiple pathways and activation of p53-up-regulated modulator of apoptosis (PUMA) and NOXA by p53. *J. Biol. Chem.,* 281, 7260–7270.
25. Reimertz, C. *et al.* (2003) Gene expression during ER stress-induced apoptosis in neurons: induction of the BH3-only protein Bbc3/PUMA and activation of the mitochondrial apoptosis pathway. *J. Cell Biol.,* 162, 587–597.
26. Breckenridge, D.G. *et al.* (2003) Regulation of apoptosis by endoplasmic reticulum pathways. *Oncogene,* 22, 8608–8618.
27. Ghaffari, S. *et al.* (2003) Cytokines and BCR-ABL mediate suppression of TRAIL-induced apoptosis through inhibition of forkhead FOXO3a transcription factor. *Proc. Natl. Acad. Sci. USA,* 100, 6523–6528.
28. Kuroda, I. *et al.* (2013) BCR-ABL regulates death receptor expression for TNF-related apoptosis-inducing ligand (TRAIL) in Philadelphia chromosome-positive leukemia. *Oncogene,* 32, 1670–1681.
29. Chu, I.M. *et al.* (2008) The Cdk inhibitor p27 in human cancer: prognostic potential and relevance to anticancer therapy. *Nat. Rev. Cancer,* 8, 253–267.
30. Woehlbier, U. *et al.* (2011) Modulating stress responses by the UPRosome: a matter of life and death. *Trends Biochem. Sci.,* 36, 329–337.
31. Rodriguez, D. *et al.* (2011) Integrating stress signals at the endoplasmic reticulum: the BCL-2 protein family rheostat. *Biochim. Biophys. Acta,* 1813, 564–574.
32. Rix, U. *et al.* (2007) Chemical proteomic profiles of the BCR-ABL inhibitors imatinib, nilotinib, and dasatinib reveal novel kinase and nonkinase targets. *Blood,* 110, 4055–4063.
33. Zhang, T. *et al.* (2012) Discovery of potent and selective covalent inhibitors of JNK. *Chem. Biol.,* 19, 140–154.
34. Waller, D.D. *et al.* (2016) A covalent cysteine-targeting kinase inhibitor of IRE1 permits allosteric control of endoribonuclease activity. *Chembiochem,* 17, 843–851.
35. Ron, D. *et al.* (2007) Signal integration in the endoplasmic reticulum unfolded protein response. *Nat. Rev. Mol. Cell Biol.,* 8, 519–529.
36. Uckun, F.M. *et al.* (2011) Inducing apoptosis in chemotherapy-resistant B-lineage acute lymphoblastic leukaemia cells by targeting HSPA5, a master regulator of the anti-apoptotic unfolded protein response signalling network. *Br. J. Haematol.,* 153, 741–752.
37. Yang, J.Y. *et al.* (2009) A new fork for clinical application: targeting forkhead transcription factors in cancer. *Clin. Cancer Res.,* 15, 752–757.
38. Consolaro, F. *et al.* (2015) FOXO3a and posttranslational modifications mediate glucocorticoid sensitivity in B-ALL. *Mol. Cancer Res.,* 13, 1578–1590.
39. Ho, K.K. *et al.* (2012) Phosphorylation of FOXO3a on Ser-7 by p38 promotes its nuclear localization in response to doxorubicin. *J. Biol. Chem.,* 287, 1545–1555.
40. Urano, F. *et al.* (2000) Coupling of stress in the ER to activation of JNK protein kinases by transmembrane protein kinase IRE1. *Science,* 287, 664–666.